A Triply [5]Helicene-Bridged (1,3,5)Cyclophane

Frédéric Aribot, Amélie Merle, Pierre Dechambenoit, Harald Bock, Albert Artigas, Nicolas Vanthuyne, Yannick Carissan, Denis Hagebaum-Reignier, Yoann Coquerel, Fabien Durola

How to cite: *Angew. Chem. Int. Ed.* **2023**, e202304058
doi.org/10.1002/anie.202304058

A Triply [5]Helicene-Bridged (1,3,5)Cyclophane

Frédéric Aribot, Amélie Merle, Pierre Dechambenoit, Harald Bock, Albert Artigas, Nicolas Vanthuyne, Yannick Carissan, Denis Hagebaum-Reignier, Yoann Coquerel, and Fabien Durola**

Dedicated to Professor Shigeru Yamago on the occasion of his 60th birthday

Abstract: A rigid propeller-shaped conjugated triple macrocycle consisting of two nearly perfectly stacked benzene rings and three linking [5]helicene moieties has been synthesized using a glyoxylic Perkin approach. Analysis of the electron delocalization in this atypical aromatic molecule revealed global aromaticity and a 78 π-electron circuit along the edge of its triple loop, to the detriment of the two 6 π-electron circuits in the two stacked benzene rings.

Introduction

Progress in the synthesis of three-dimensional π-conjugated macrocycles has been considerable in recent years,[1] introducing new systems for host–guest chemistry[2,3] and allowing new insights into the concept of aromaticity.[1,4] Among the many examples of 3D conjugated macrocycles[5–7] reported recently, conjugated hydrocarbons have been a rarity since the introduction of the nanoball by Itami[8] and Yamago.[9] Amid the newer examples, some interesting radical behavior[10] and distorted [5]helicene structures[11] have been reported (Figure 1). Either by design or because of the difficulty of their synthesis, 3D conjugated hydrocarbon macrocycles presenting intramolecular π–π interactions remain elusive entities as most reported examples contain rather big cavities.

Cases of destabilizing π–π interactions are rarely observed[12] because most aromatic systems adopt a slipped-stack structure to minimize the electrostatic repulsion between π-electrons.[13] This escape route can be blocked by forcing both rings to face each other with structural rigidity. One well-studied example is the simple [2,2]paracyclophane (Figure 2a), showing considerable repulsion between the two benzene rings which are particularly close (3.09 Å) and bend to adopt a boat conformation in response to this repulsion.[14] Recently Matsuda's group reported a homologous compound[15] to [2,2]paracyclophane (Figure 2b) where the two central benzene rings adopt preferentially a slipped tilted conformation (with an interplanar angle of 18.1°) due to insufficient rigidity and ring tension.

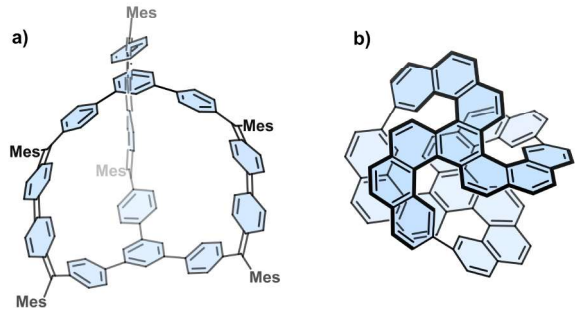

Figure 1. Wu's (a) and Watanabe's (b) recent three-dimensional conjugated hydrocarbon macrocycles.

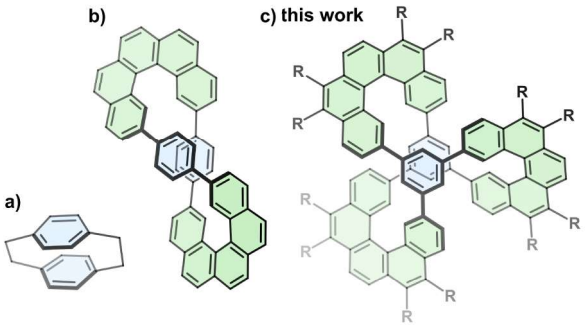

Figure 2. Molecular architectures with stacked benzene rings (in blue). a) slipped stacked in [2,2]paracyclophane, b) slipped tilted in Matsuda's double propeller and c) nearly perfectly stacked in this article's triple propeller (R = CO_2Et).

Results and Discussion

Our group has developed a versatile synthetic approach for the formation of large carboxy-substituted polycyclic aromatic compounds,[16] which turned out to be very efficient for the formation of macrocycles,[17,18] especially [5]helicene-

[*] Dr. F. Aribot, A. Merle, Dr. P. Dechambenoit, Dr. H. Bock, Dr. F. Durola
Centre de Recherche Paul Pascal – CNRS & Univ. Bordeaux
115 Ave. du Dr. Schweitzer, 33600 Pessac (France)
E-mail: fabien.durola@crpp.cnrs.fr
Dr. A. Artigas, Dr. N. Vanthuyne, Dr. Y. Carissan, Dr. D. Hagebaum-Reignier, Dr. Y. Coquerel
Aix Marseille Univ., CNRS, Centrale Marseille, iSm2
Marseille (France)
E-mail: yoann.coquerel@univ-amu.fr

containing rigid conjugated macrocycles.[19,20] This synthetic strategy relies on the assembly of arylacetic and arylglyoxylic acids by Perkin condensation reactions, which leads to flexible precursors composed of aromatic fragments linked together by maleic (imide or diester) bridges. A Mallory photocyclisation of these flexible precursors has afforded a wide variety of carboxy-substituted arenes.[19–22] To take advantage of this, a new trifunctional building block suitable for Perkin reactions has been designed, and a compound composed of two benzene units triply linked together by three [5]helicene bridges has been targeted (Figure 2c). Initial computational modeling of this molecule revealed a very rigid D_3-symmetric structure with both trisubstituted benzene central rings perfectly stacked on top of each other and not exhibiting any degree of freedom. This alignment and proximity of both central benzene rings (with an average interplanar distance of 3.6 Å) and the overall rigidity of the system may translate into unusual aromaticity.[23,24]

Herein we present the synthesis of this triply [5]helicene-bridged (1,3,5)cyclophane **G** (Scheme 1), its structural elucidation by single crystal X-ray diffraction analysis, the resolution of its enantiomers, the determination of its (chir)optical properties, and a study of electron delocalization and aromaticity in a model compound **H**.

Among the different ways to introduce glyoxylic functions onto an aromatic substrate, direct lithium-halogen exchange followed by addition of a dialkyl oxalate appears to be the most versatile and efficient approach, as it usually affords the desired product in high yields on the gram scale. It can be done on bromoaryl substrates of various sizes and shapes, and we demonstrate here that introducing up to three glyoxylic functions simultaneously is possible: 1,3,5-tris(4-bromophenyl)benzene **A** was obtained in 72 % yield from commercially available 4-bromoacetophenone by trimerization in the presence of thionyl chloride in ethanol,[25] and **A** then underwent threefold lithium-bromide exchange with ^{t}BuLi at −94 °C to form the corresponding trilithiated intermediate, which then reacted in situ with an excess of diethyl oxalate to give the expected triethyl 1,3,5-triphenylbenzene-4′,4″,4‴-triglyoxylate **B** in 81 % yield after precipitation from ethanol. Quantitative saponification of **B** with sodium bicarbonate afforded 1,3,5-triphenylbenzene-4′,4″,4‴-triglyoxylic acid **C** as a first trifunctional building block for the glyoxylic Perkin reaction. Triglyoxylic acid **C** was then condensed with three equivalents of 1,4-benzenediacetic acid monomethyl ester[18] **II** in a triple Perkin reaction. Due to the non-reactivity of areneacetic esters in Perkin conditions,[26] the monoprotection of benzenediacetic acid as monoester allows us to tailor extended aromatic systems by sequential Perkin reactions. The mono-ester **II** was obtained from the statistical saponification of 1,4-benzenediacetic dimethyl ester **I**. Three equivalents of **II** were then condensed with triglyoxylic acid **C** in a triple Perkin reaction, followed by the usual in situ esterification in order to simplify purification, to yield the flexible nona-ester **D** in 48 % yield. A swift saponification of **D** with excess KOH in a mixture of ethanol and water then afforded quantitatively

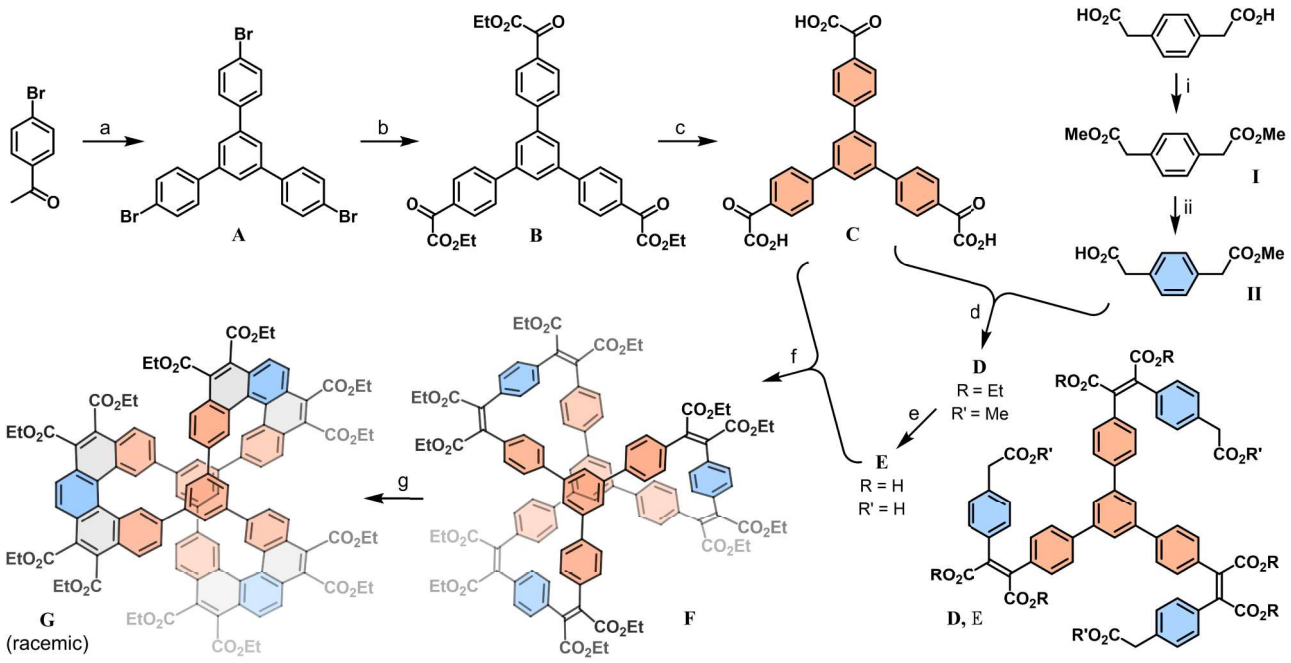

Scheme 1. Synthesis of the D_3 symmetric tris[5]helicenylene-cyclophane **G**: a) $SOCl_2$, EtOH, reflux, 1 h, 72 %; b) ^{t}BuLi followed by $(EtO_2C)_2$, THF, −94 °C, 4 h, 81 %; c) $NaHCO_3$, H_2O-EtOH, reflux 15 h, quant.; d) NEt_3, Ac_2O, THF, reflux 15 h, followed by addition of EtOH, EtBr, DBU, reflux 15 h, 48 %; e) KOH, H_2O-EtOH, reflux 15 h, quant.; f) NEt_3, Ac_2O, THF, high dilution conditions (see end of caption), reflux, 64 h, followed by addition of EtOH, EtBr, DBU, reflux 15 h, 33 % g) I_2, AcOEt, *hν*, rt, 48 h, 62 % (1) $SOCl_2$, MeOH, reflux, 3 h, 98 % (2) KOH, dioxane-MeOH, reflux 15 h, 32 %. High dilution conditions: 0.47 mmol of both substrates were dissolved in about 50 mL of THF and added dropwise over 24 h (about 2 mL h^{-1}) to the reaction mixture (1 L) using a syringe pump.

the corresponding flexible nona-acid **E**, which contains three Perkin-reactive acetic acid functions and six inert non-enolisable carboxylic acid moieties. Both macrocycle precursors—i.e. the triacetic acid **E** and the triglyoxylic acid **C**—were then condensed together by a triple (once inter- and twice intra-molecular) Perkin reaction, where the high dilution conditions were controlled by the automated slow addition of the two substrates to the reaction medium. The desired racemic flexible macrocyclic compound **F** was thus obtained with a very satisfying yield of 33 %. Finally, **F** was rigidified through a six-fold Mallory cyclization in ethyl acetate in the presence of iodine and oxygen over two days with pyrex-filtered light from a medium pressure mercury lamp. After precipitation from ethanol, the racemic final product **G** was obtained as a single diastereomer and fully characterized by NMR spectroscopy. Single crystals of **G** suitable for X-ray diffraction were obtained by slow diffusion of cyclohexane into a solution of chloroform.[27] The crystal structure shows non-slipped parallel stacking of the two central rings, which, as expected from our initial simulations, are separated by an average distance of 3.6 Å (Figure 3). Notably, the twelve dihedral angles along the six C–C single bonds radiating from the central rings were measured at 3.3 to 23.4° with an average value of 9.8°.

The triple macrocycle **G** contains six stereogenic axes along the single bonds radiating from the central phenyl rings and three stereogenic [5]helicene units. Despite the existence of nine stereogenic elements in this molecule, it can only exist as a single diastereomer and it can reasonably be assumed that its enantiomerization is impossible for geometric reasons. The resolution of the enantiomers of the triple macrocycle **G** was achieved using preparative HPLC to obtain enantiopure samples (>99 % *ee*, see the Supporting Information). The two enantiomers of **G** show identical absorption and fluorescence spectra (Figure 4, top) with a maximum absorbance at 263 nm ($\varepsilon \approx 217\times10^3\ M^{-1}cm^{-1}$), and a weak fluorescence under excitation at 355 nm showing a maximum emission at 455 nm ($\Phi f = 0.068$, see Figure S6). The absorption spectrum of **G** is comparable with the absorption spectrum of the isolated [5]helicene tetraester,[28] with an approximate three-fold enhancement in intensity

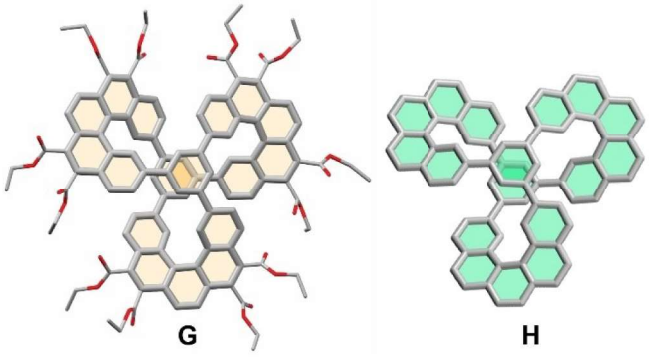

Figure 3. Left: Crystal structure of **G**. Right: Simplified version **H**, lacking the ester groups, used for the evaluation of aromaticity. Hydrogen atoms have been omitted for clarity.

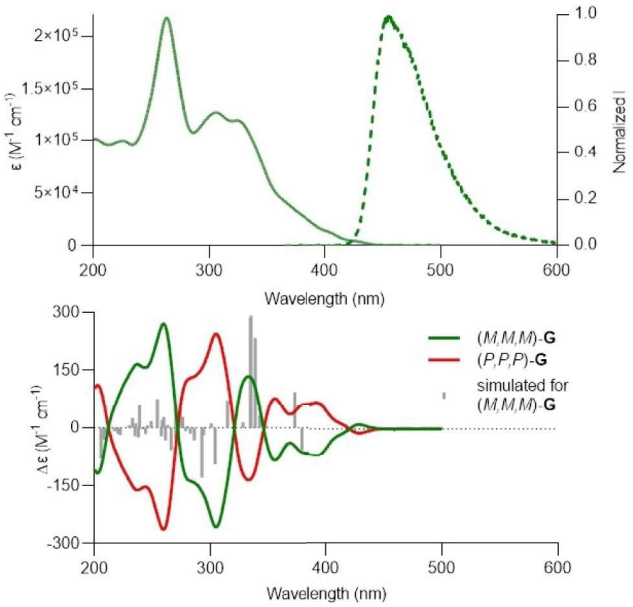

Figure 4. Top: Absorption (continuous) and emission (dashed, $\lambda_{ex}=355$ nm) spectra of (*M*,*M*,*M*)-**G**. Bottom: ECD spectra of both enantiomers of **G** (green = first eluted, red = second eluted); the gray bars show the TD-DFT-derived rotatory strength values computed for (*M*,*M*,*M*)-**G**. See the Supporting Information for details.

and a global redshift of ca. 40 nm. Mirror ECD spectra were recorded for the enantiomers of **G** (Figure 4, bottom), with an absorptive dissymmetry factor $|g_{abs}| = 1.1\times10^{-3}$ at 263 nm and a maximum $|g_{abs}| = 4.0\times10^{-3}$ at 396 nm. These values of $|g_{abs}|$ are comparable in magnitude, but with variations in wavelengths, with the ones for pristine [5]helicene ($|g_{abs}| = 4.2\cdot10^{-3}$ at 310 nm)[29] and for the isolated [5]helicene tetraester ($|g_{abs}| = 4.6\times10^{-3}$ at 212 nm).[28] The observed Cotton effects for the second eluted enantiomer of **G**, negative around 263 nm and positive around 306 nm, parallel the ones of pristine (*P*)-[5]helicene and related multiple helicenes.[30] Comparison of the experimental ECD spectra with the simulated spectrum obtained by TD-DFT for the (*M*,*M*,*M*) enantiomer confirmed the absolute configuration as (*M*,*M*,*M*)-**G** for the first eluted enantiomer and (*P*,*P*,*P*)-**G** for the second eluted enantiomer (Figure 4, bottom). The specific optical rotations are $[\alpha]_D^{25} = +800\ deg\,mL\,g^{-1}\,dm^{-1}$, $[\alpha]_{578}^{25} = +855\ deg\,mL\,g^{-1}\,dm^{-1}$, and $[\alpha]_{546}^{25} = +1070\ deg\,mL\,g^{-1}\,dm^{-1}$ for (*P*,*P*,*P*)-**G** (*c* 0.20, dichloromethane), and opposite values were recorded for (*M*,*M*,*M*)-**G** (*c* 0.19, dichloromethane). In comparison, the specific rotation for pristine (*P*)-[5]helicene is $[\alpha]_D^{25} = +2760\ deg\,mL\,g^{-1}\,dm^{-1}$ (*c* 0.013, *n*-hexane:2-propanol),[29] and the one for (*P*)-configured isolated [5]helicene tetraester is $[\alpha]_D^{25} = +680\ deg\,mL\,g^{-1}\,dm^{-1}$ (*c* 0.090, dichloromethane).[28]

To evaluate the aromaticity in **G**, a simplified version with all ester groups replaced by H atoms was optimized without symmetry constraints by DFT methods (**H**, D_3-symmetry, see Figure 3, right). Electron delocalization and aromaticity in **H** were evaluated on the basis of magnetic and electronic criteria.[31,32] At first, the 3D isotropic magnetic shielding (IMS) isocontour map[33] of **H** was

generated (Figure 5a; the 3D IMS contour map of **H** is interactive and is available for visualization and personalization in the Supporting Information as a .vtk file). The IMS isocontours were plotted on a surface made of overlapping 1 Å radius spheres around all atoms including some artificially introduced dummy atoms at specific positions, as previously described.[33] Interpretation of the 3D IMS isocontour map is intuitive: color becomes darker with an increase of the absolute value of IMS, with blue indicating an aromatic character (positive IMS induced by diatropic currents), and red indicating an antiaromatic character (negative IMS induced by paratropic currents). Dark blue areas indicate relatively intense delocalization, and continuous dark blue rings reminiscent of Clar π-sextets indicate plain aromaticity as in benzene (see examples in Figure S10). Because of the D_3-symmetry, the three [5]helicene units in **H** are equivalent and so are both faces of the molecule. However, the two faces of each ring are not magnetically equivalent and show different inner and outer IMS values. By comparing the 3D IMS isocontours of the [5]helicene units in **H** with the 3D IMS isocontours of pristine [5]helicene (see Figure S10), one can note a global decrease of the aromaticity visualized by smaller dark blue areas in the [5]helicene units of **H**, but the overall delocalization patterns are comparable. In contrast, comparing the 3D IMS isocontours of the two central six-membered rings with the 3D IMS isocontours of benzene revealed dramatic differences, particularly visible on the convex face of the two central six-membered rings in **H** that show only sharp dark blue areas located over the six C–C bonds (Figure 5a). Two hypotheses were examined to account for this observation. First, the effect of the perfect stacking between the two central six-membered rings was considered. However, it could be verified it is not the case using a model perfectly stacked benzene dimer (see Supporting Information, Figure S7 and the corresponding text). Next, we hypothesized that the particular geometry of the two 1,3,5-triarylbenzene units could be at the origin of the observed IMS isocontour pattern. Model 1,3,5-triphenylbenzene optimized without any constraints, does not show the same pattern as **H**. In this case, a continuous star-shaped dark blue area is visible on both faces, indicating relatively intense circular 6π electron delocalization over this ring (Figure 5b). Conversely, when imposing the geometry of **H** to the same model, an identical pattern to that of **H** was obtained (Figure 5c), confirming the second hypothesis.

In parallel, a comparative examination of the electron density of delocalized double bonds (EDDB(r))[34] in **H** and its 1,3,5-triphenylbenzene models was performed (Figure 6). EDDB(r) is easy to interpret: the greater the volume of the isosurface over bonds, the greater the delocalization over these bonds. Similarly, the higher is the obtained value of |e|, the more aromatic is the system. While a discontinuous isosurface is obtained over the convex faces of **H** and its constraint model, their concave faces show a continuous isosurface indicating enhanced ring-to-ring delocalization through the single bonds (Figure 6a and c). Both equivalent faces of the unconstraint model show discontinuities (Figure 5b). Such ring-to-ring delocalization over the concave face may explain the original pattern observed over the convex face of the 3D IMS map and points out for the existence of a global circuit for delocalization in this molecule.

The two central six-membered rings in **H** are nearly planar and parallel to each other, and the other six-membered rings in **H** only moderately deviate from this plane. Therefore, anisotropic current density analyses (CDA) could be performed, with the applied magnetic field oriented perpendicular to the mean plane defined by the six C atoms of the central rings. Using the CDA option available in the AICD software,[35,36] the induced current

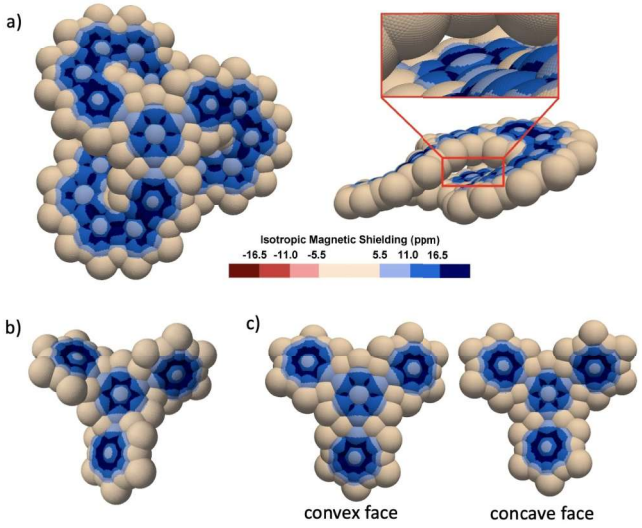

Figure 5. 3D IMS isocontour map of **H** (a), of 1,3,5-triphenylbenzene (b), and of 1,3,5-triphenylbenzene constrained in the geometry of **H** (c).

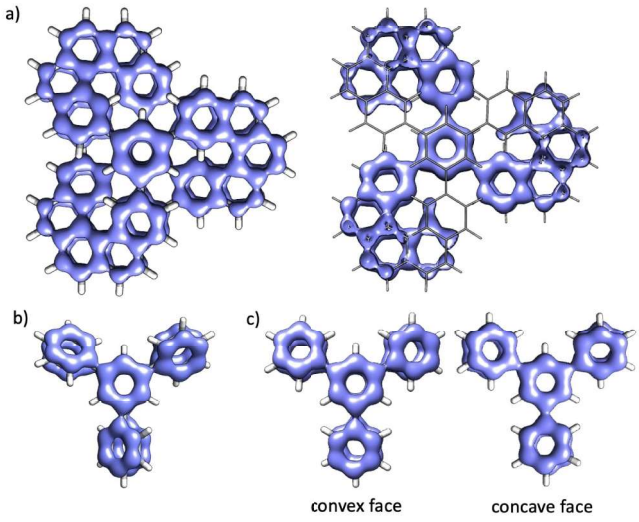

Figure 6. Representations of EDDBH(r) isosurfaces using an isovalue of 0.02, and EDDBH(r) values for a) **H** (0.8040|e|=/atom), b) 1,3,5-triphenylbenzene (0.9594|e|/atom), and c) 1,3,5-triphenylbenzene constrained in the geometry of **H** (0.9630|e|/atom). |e|=delocalized electrons.

density in **H** could be plotted as vectors onto the AICD isosurface (Figure 7a). It can be observed that the induced electron flow is significant along the external rim (diatropic current) and along internal rim (paratropic current) of the three [5]helicene units. There is seemingly a circular electron flow over the two central six-membered rings (only the convex face is visible in Figure 7a) but it can also be observed that some current densities are escaping or joining the central six-membered ring along the three C(sp^2)–C(sp^2) single bonds radiating from it (zoom in the red square in Figure 7a). To get a clear picture of the preferred direction of the induced currents when a magnetic field is applied to **H** perpendicularly to its mean molecular plane, the induced currents were visualized with the GIMIC software[37,38] (Figure 7b). From this analysis, it can be inferred that a significant global 78 π-electron circuit for delocalization exists in **H**, to the detriment of circular 6π delocalization in the central six-membered rings. In the global 78 π-electron circuit, the π system in the central six-membered rings is acting as a three-fold relay between neighboring [5]helicene units. The global circuit is as follows: Starting from the red dot shown on the AICD + CDA visualization (Figure 7a), the electron flow goes diatropically through two C–C bonds of the top central six-membered ring and then leaves the central ring to continue diatropically on the external rim of the closest [5]helicene unit (at right in the picture) until it reaches the bottom central six-membered ring. From there, the electron flow is continuing diatropically through two C–C bonds of the bottom central six-membered ring and then paratropically on the internal rim of the closest [5]helicene unit (bottom left in the picture) until it reaches the upper central six-membered ring again, now at the blue dot. From there, two additional loops around the edge of the structure would complete the circuit, allowing to come back to the red dot (see the Supporting Information Figure S9 for a complementary visualization of the circuit). From the Hückel point of view, this 78-π-electron circuit would be aromatic as it obeys the 4n + 2 rule.

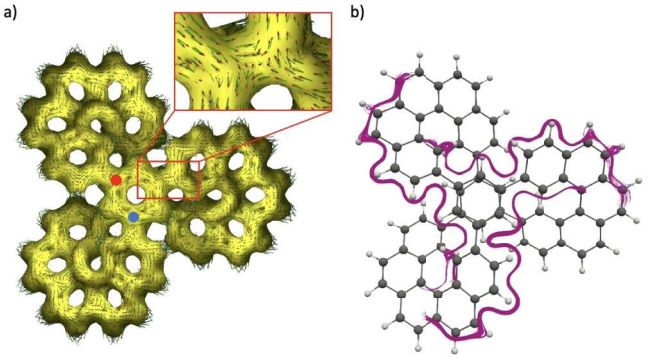

Figure 7. Current Density Analysis (CDA) of **H** using (a) the Anisotropy of the Induced Current Density (AICD) isosurface with isovalue = 0.03 to plot the vectors, and (b) the Gauge Independent Magnetically Induced Currents (GIMIC) with three symmetric seed spheres for best visualization. The external applied magnetic field is pointing toward the observer. Diatropic currents correspond to clockwise circulation of electrons, paratropic currents to counterclockwise circulation.

Conclusion

In conclusion, the synthesis of a triply [5]helicene-bridged (1,3,5)cyclophane **G** was efficiently accomplished via the Perkin-reaction-based strategy developed by the Durola group for the formation of large carboxy-substituted polycyclic aromatic compounds. The synthesis of **G** features a particularly challenging threefold Perkin olefination / Mallory cyclisation sequence, highlighting the usefulness of this approach for the synthesis of severely constrained molecules. Despite the presence of six single C–C bonds, the aromatic entity is very rigid and does not have any conformational freedom. Significantly, the two central phenyl rings in **G** are parallel and near-perfectly stacked at a 3.6 Å distance. The enantiomers of **G** exhibited (chir)optical properties characteristic of molecules containing [5]helicene moieties. The investigation of electron delocalization and aromaticity in **H**, a simplified version of **G** with ester groups replaced by hydrogen atoms, revealed a global aromatic character of the molecule and the existence of a 78 π-electron circuit along the edge of the molecule that passes through each of the six C(sp^2)–C(sp^2) single bonds in both opposite directions.

Acknowledgements

F.A. thanks the University of Bordeaux for a Ph.D. grant. A.A. thanks the Spanish Ministerio de Universidades and the E.U. for a Margarita Salas post-doctoral fellowship. This work was funded, in part, by the French Agence Nationale de la Recherche—ANR (ANR-19-CE07-0041). We thank Ms Marion Jean (Aix-Marseille Univ) for assistance with chiral HPLC, and Mr Florian Rigoulet (Aix-Marseille Univ) for assistance with fluorescence spectroscopy. We are grateful to the CNRS, Aix Marseille University and the University of Bordeaux for support.

Conflict of Interest

The authors declare no conflict of interest.

Data Availability Statement

The data that support the findings of this study are available from the corresponding author upon reasonable request.

Keywords: Aromaticity · Cyclophane · Helicene · Macrocycle · Perkin Reaction

[1] O. El Bakouri, D. W. Szczepanik, K. Jorner, R. Ayub, P. Bultinck, M. Solà, H. Ottosson, *J. Am. Chem. Soc.* **2022**, *144*, 8560.

[2] X. S. Ke, T. Kim, Q. He, V. M. Lynch, D. Kim, J. L. Sessler, *J. Am. Chem. Soc.* **2018**, *140*, 16455.

[3] S. Cui, G. Zhuang, D. Lu, Q. Huang, H. Jia, Y. Wang, S. Yang, P. Du, *Angew. Chem. Int. Ed.* **2018**, *57*, 9330.
[4] G. Merino, M. Solà, I. Fernandez, C. Foroutan-Nejad, P. Lazzeretti, G. Frenking, H. L. Anderson, D. Sundholm, F. P. Cossio, M. A. Petrukhina, J. Wu, J. I. Wu, A. Restrepo, *Chem. Sci.* **2023**, *14*, https://doi.org/10.1039/d2sc04998h.
[5] J. Zhu, Y. Han, Y. Ni, S. Wu, Q. Zhang, T. Jiao, Z. Li, J. Wu, *J. Am. Chem. Soc.* **2021**, *143*, 14314.
[6] A. Basavarajappa, M. D. Ambhore, V. G. Anand, *Chem. Commun.* **2021**, *57*, 4299.
[7] N. Hayase, J. Nogami, Y. Shibata, K. Tanaka, *Angew. Chem. Int. Ed.* **2019**, *58*, 9439.
[8] K. Matsui, Y. Segawa, T. Namikawa, K. Kamada, K. Itami, *Chem. Sci.* **2012**, *3*, 84.
[9] E. Kayahara, T. Iwamoto, H. Takaya, T. Suzuki, M. Fujitsuka, T. Majima, N. Yasuda, N. Matsuyama, S. Seki, S. Yamago, *Nat. Commun.* **2013**, *4*, 2694.
[10] Y. Ni, F. Gordillo-Gámez, M. Peña Alvarez, Z. Nan, Z. Li, S. Wu, Y. Han, J. Casado, J. Wu, *J. Am. Chem. Soc.* **2020**, *142*, 12730.
[11] T. Matsushima, S. Kikkawa, I. Azumaya, S. Watanabe, *ChemistryOpen* **2018**, *7*, 278.
[12] R. Nozawa, H. Tanaka, W. Y. Cha, Y. Hong, I. Hisaki, S. Shimizu, J. Y. Shin, T. Kowalczyk, S. Irle, D. Kim, H. Shinokubo, *Nat. Commun.* **2016**, *7*, 13620.
[13] C. R. Martinez, B. L. Iverson, *Chem. Sci.* **2012**, *3*, 2191.
[14] Z. Hassan, E. Spuling, D. M. Knoll, S. Bräse, *Angew. Chem. Int. Ed.* **2020**, *59*, 2156.
[15] H. Kubo, D. Shimizu, T. Hirose, K. Matsuda, *Org. Lett.* **2020**, *22*, 9276.
[16] L. Sturm, F. Aribot, L. Soliman, H. Bock, F. Durola, *Eur. J. Org. Chem.* **2022**, e202200196.
[17] A. Robert, P. Dechambenoit, H. Bock, F. Durola, *Can. J. Chem.* **2017**, *95*, 450.
[18] G. Naulet, A. Robert, P. Dechambenoit, H. Bock, F. Durola, *Eur. J. Org. Chem.* **2018**, 619.
[19] A. Robert, P. Dechambenoit, E. A. Hillard, H. Bock, F. Durola, *Chem. Commun.* **2017**, *53*, 11540.
[20] G. Naulet, L. Sturm, A. Robert, P. Dechambenoit, F. Röhricht, R. Herges, H. Bock, F. Durola, *Chem. Sci.* **2018**, *9*, 8930.
[21] H. Bock, D. Subervie, P. Mathey, A. Pradhan, P. Sarkar, P. Dechambenoit, E. A. Hillard, F. Durola, *Org. Lett.* **2014**, *16*, 1546.
[22] T. S. Moreira, M. Ferreira, A. Dall'armellina, R. Cristiano, H. Gallardo, E. A. Hillard, H. Bock, F. Durola, *Eur. J. Org. Chem.* **2017**, 4548.
[23] M. Orozco-Ic, R. R. Valiev, D. Sundholm, *Phys. Chem. Chem. Phys.* **2022**, *24*, 6404.
[24] I. Majerz, T. Dziembowska, *J. Phys. Chem. A* **2016**, *120*, 8138.
[25] S. Kanti Das, S. Mishra, K. Manna, U. Kayal, S. Mahapatra, K. Das Saha, S. Dalapati, G. P. Das, A. A. Mostafa, A. Bhaumik, *Chem. Commun.* **2018**, *54*, 11475.
[26] G. Naulet, S. Huet-Exiga, H. Bock, F. Durola, *Org. Chem. Front.* **2019**, *6*, 994.
[27] Deposition Number 2215761 contains the supplementary crystallographic data for this paper. These data are provided free of charge by the joint Cambridge Crystallographic Data Centre and Fachinformationszentrum Karlsruhe Access Structures service.
[28] A. Robert, G. Naulet, H. Bock, N. Vanthuyne, M. Jean, M. Giorgi, Y. Carissan, C. Aroulanda, A. Scalabre, E. Pouget, F. Durola, Y. Coquerel, *Chem. Eur. J.* **2019**, *25*, 14364.
[29] Y. Nakai, T. Mori, Y. Inoue, *J. Phys. Chem. A* **2012**, *116*, 7372.
[30] T. Mori, *Chem. Rev.* **2021**, *121*, 2373.
[31] *Aromaticity: Modern Computational Methods and Applications* (Ed.: I. Fernández), Elsevier, Amsterdam, **2021**.
[32] *Aromaticity and Antiaromaticity: Concepts and Applications* (Eds.: M. Solà, A. I. Boldyrev, M. K. Cyrañski, T. M. Krygowski, G. Merino), Wiley-VCH, Weinheim, **2022**.
[33] A. Artigas, D. Hagebaum-Reignier, Y. Carissan, Y. Coquerel, *Chem. Sci.* **2021**, *12*, 13092.
[34] D. W. Szczepanik, M. Andrzejak, J. Dominikowska, B. Pawełek, T. M. Krygowski, H. Szatylowicz, M. Solà, *Phys. Chem. Chem. Phys.* **2017**, *19*, 28970.
[35] R. Herges, D. Geuenich, *J. Phys. Chem. A* **2001**, *105*, 3214.
[36] D. Geuenich, K. Hess, F. Köhler, R. Herges, *Chem. Rev.* **2005**, *105*, 3758.
[37] J. Jusélius, D. Sundholm, J. Gauss, *J. Chem. Phys.* **2004**, *121*, 3952.
[38] H. Fliegl, S. Taubert, O. Lehtonen, D. Sundholm, *Phys. Chem. Chem. Phys.* **2011**, *13*, 20500.

Manuscript received: March 21, 2023
Accepted manuscript online: May 11, 2023
Version of record online: ■■, ■■